



6-18-2018

## Reconsidering downwind operation by analysis of the NREL Phase VI data

Scott Larwood

*University of the Pacific*, slarwood@pacific.edu

Raymond Chow

*Rescale Inc.*

Follow this and additional works at: <https://scholarlycommons.pacific.edu/soecs-facarticles>



Part of the [Engineering Commons](#), and the [Environmental Sciences Commons](#)


---

### Recommended Citation

Larwood, S., & Chow, R. (2018). Reconsidering downwind operation by analysis of the NREL Phase VI data. *Wind Engineering*, , 1–13. DOI: [10.1177/0309524X18780387](https://doi.org/10.1177/0309524X18780387)  
<https://scholarlycommons.pacific.edu/soecs-facarticles/76>

This Article is brought to you for free and open access by the All Faculty Scholarship at Scholarly Commons. It has been accepted for inclusion in All Faculty Articles - School of Engineering and Computer Science by an authorized administrator of Scholarly Commons. For more information, please contact [mgebney@pacific.edu](mailto:mgebney@pacific.edu).

# Reconsidering downwind operation by analysis of the NREL Phase VI data

Journal Title  
XX(X):1–13  
©The Author(s) 2018  
Reprints and permission:  
sagepub.co.uk/journalsPermissions.nav  
DOI: 10.1177/ToBeAssigned  
www.sagepub.com/  


Scott Larwood<sup>1</sup> and Raymond Chow<sup>2</sup>

## Abstract

Data are presented comparing upwind versus downwind operation of the National Renewable Energy Laboratory's Phase VI wind turbine. Power was not reduced as expected for downwind, which may be attributed to inboard three-dimensional effects. Average flap bending loads were reduced with downwind coning and compared well with prediction. Fatigue loads were increased with downwind; however, fatigue was mitigated with a tower shroud. The shroud needs to align with the freestream, demonstrated by an increase in fatigue loads from a 10° shroud misalignment. Pressure data were acquired in the tower wake at the rotor location with and without the shroud. The bare-tower wake data compared well with previous work. The shroud wake data at 10° and 20° misalignment showed velocity reduction and turbulence exceeding the bare tower values. Downwind operation, with an aligning tower shroud, should be considered for future designs given the load benefits of downwind coning.

## Keywords

downwind turbines, tower wake, rotor-tower interaction, wind tunnel testing, coning

## Introduction

The predominant wind turbine configuration is horizontal-axis, three-bladed, upwind rotors (rotor upwind of tower). Several large downwind research turbines were constructed in the past; examples of these in the United States were the 100 kW MOD-0 (Glasgow et al. 1981) and the Hamilton Standard 4 MW WTS-4 (Spera 2009), which were U.S. government-sponsored research projects in response to the energy crises of the 1970's. Smaller downwind turbines available commercially in the 1980's were the 80 kW ESI-80 and the 25 kW Carter (Gipe 1995). Downwind turbines have the potential for lower average blade and yawing loads and thus lower mass/cost. The design also effectively removes the constraint of blade tip clearance with the tower. However, problems such as fatigue and noise arise from the rotor interacting with the tower wake. Recent advances in offshore wind energy, including turbines on floating platforms, has renewed interest in large downwind designs that can be placed far from shore. Ichter et al. (2016) and Loth et al. (2017) present a large downwind concept, which was the inspiration for this writing.

This paper reports on unpublished data from the National Renewable Energy Laboratory's (NREL) Unsteady Aerodynamics Experiment (UAE) Phase VI (Hand et al.

2001) which was obtained at the National Full-Scale Aerodynamics Complex 80- by 120-foot wind tunnel at NASA Ames Research Center. The prior UAE literature was focused on model validations and not comparison between upwind and downwind operation. For example, Coton et al. (2002) report on modeling (prescribed wake) for the downwind cases in the UAE Phase VI data. They found that the modeling results were highly dependent on the wake model, which included a wake width and velocity deficit. They also report on a phase difference between the measurements and the modeling, which was suspected to be a rotor-tower wake interaction. This seemed to be confirmed in the modeling results (RANS) of Zahle et al. (2009).

Experimental comparisons between upwind and downwind operation have been rare. Glasgow et al. (1981) report on upwind and downwind operation of the MOD-0 (unconed). Mean blade bending moments were found to be the same, but cyclic moment showed an increasing

<sup>1</sup>University of the Pacific, CA, USA

<sup>2</sup>Rescale Inc., San Francisco, CA, USA

## Corresponding author:

Scott Larwood, University of the Pacific Mechanical Engineering Department, 3601 Pacific Ave, Stockton, CA 95211 USA.

Email: slarwood@pacific.edu

trend with wind speed for downwind operation. Power measurements were not available for this experiment. Yoshida (2006) reports on a 100 kW turbine configured for upwind and downwind operation. Power was increased 7-10% in downwind operation, which was attributed to a favorable combination of sloping terrain and shaft tilt. Water-channel experiments by Kress et al. (2015) showed higher power for downwind compared to upwind operation, which was attributed to favorable nacelle-flow confirmed in modeling by Frau et al. (2015).

This paper addresses power and load differences between upwind and downwind operation, in addition to potential benefits from a tower aerodynamic shroud (fairing). The shroud was included in the experiment to study mitigating the tower wake. Tower wake measurements, with and without the shroud, will also be presented and compared to previous research. Previous research on tower wakes were from wind tunnel studies by Snyder and Wentz (1981) and Powles (1983). While Powles studied the wake of a 12-sided polygon, Snyder and Wentz also studied the polygon in addition to a cylinder and a cylinder with strakes. Wilmshurst et al. (1985) added an aerodynamic shroud to the tower in further work. O'Connor et al. (2013) reported on a self-aligning fairing design for wind turbine towers, with later experimental studies (O'Connor et al. 2015).

## Methods

The NREL Unsteady Aerodynamics Experiment Phase VI wind turbine was 2-bladed with a 10 meter diameter (Figure 1). The test was conducted at the NASA-Ames 24.4- by 36.6-m (80- by 120-foot) wind tunnel. The tunnel is the largest in the world and the error due to blockage from the turbine was determined to be less than 2% for all conditions (Hand et al. 2001). The turbine could be operated in upwind or downwind mode, with adjustable blade coning. For the results presented in this paper, the coning was  $0^\circ$  for upwind operation and  $3.4^\circ$  (downwind) for downwind operation. These coning angles were maintained during the test over concerns of loading and stability (Simms et al. 1999). The teeter degree-of-freedom was fixed for upwind operation and free for downwind operation. There was an upwind sequence with teeter; however, the loads/power below rated were similar to fixed teeter. The fixed pitch, stall regulated rotor was operated at a constant 72 rpm. Most of the comparisons in this paper are made at wind speeds below rated to avoid the complication of blade stall. Turbine and tunnel data was acquired at 521 Hz and most data points represent 30 seconds of data (36 rotor revolutions). Blade loads were



**Figure 1.** UAE in upwind configuration. NASA image.

obtained with strain gage bridges which were calibrated in the tunnel. Blade surface pressures were also measured at various radial positions. One of the blades was equipped with five-hole pitot-tube probes at various radial positions to determine blade angles and velocities. Tower wake data was acquired by positioning the blade instrumented with the probes downstream of the tower (Figure 2).

Both blade loads and tower wake data were obtained with and without a tower aerodynamic shroud installed to investigate mitigating adverse effects of the tower wake. The tower diameter in the rotor swept area was a constant 0.4064 m. The maximum thickness of the symmetric shroud was 0.46 m with a 0.89 m chord length. The shroud coordinates are included in the supplemental material. The shroud was installed with plywood ribs attached to the tower. Aluminum sheets were bent around the ribs with a finite seam at the nominally-sharp trailing edge.

Note that a formal uncertainty analysis was not performed on the test; however, the expected accuracy of the data was within 1% given the calibration procedures and data review Simms et al. (2001). For most plots in this article, the measurement uncertainty would be less than the marker size.

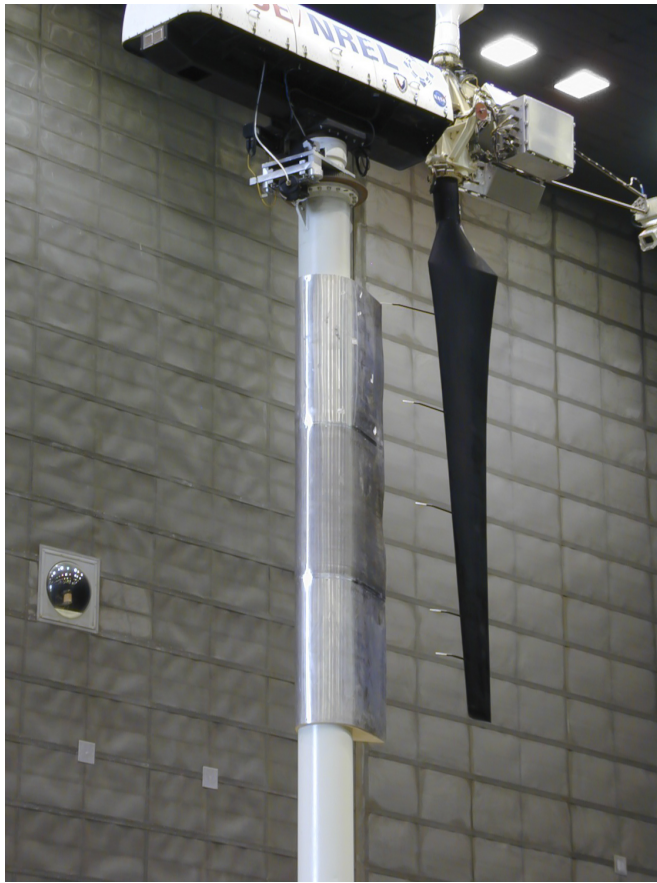


**Figure 2.** Tower shroud with instrumented blade positioned downwind for wake measurements. Photo by Lee Fingersh, NREL 36813

**Table 1.** UAE test sequences.

Sequence	Description
B	Downwind operation
H	Upwind operation
3	Tower wake measurements
6	Tower shroud measurements
7	Downwind operation with shroud

Table 1 lists the test sequences that were used in this study. Further details of the test campaign are available in [Hand et al. \(2001\)](#).

## Results and Discussion

### Power and Loads

Figure 3a shows comparison of downwind versus upwind average power for the full range of wind speeds. With downwind operating at  $3.4^\circ$  coning, one would expect a lower power due to reduced rotor swept-area (0.35%) and loss due to tower shadow. However, the annual energy production (AEP) for downwind operation is over 2% greater than upwind operation for all IEC wind classes (Rayleigh wind speed distribution) with this power curve. Figure 3b focuses on below-rated wind speeds, and downwind shows

higher power except at the highest wind speed on the plot (9.3 m/s). In this range, the downwind AEP is 10% higher than upwind. The higher downwind power can be investigated with Figure 4, which shows a comparison of averaged spanwise aerodynamic performance between the upwind and downwind operation at 5 m/s, well below the rated speed of 10 m/s. Downwind torque coefficient is higher inboard compared to upwind, as shown in Figure 4a. Downwind also shows higher inboard normal force (Figure 4b) and tangential force coefficient (Figure 4c). However, the local angle of attack is lower for downwind (Figure 4d); for example,  $\alpha = 4.4^\circ$  compared to  $5.2^\circ$  at 91% radius. The spanwise angle (angle between local chord line and relative wind speed vector) is higher for the downwind case (Figure 4e). The pressure coefficient ( $c_p$ ) at the 30% station and  $0^\circ$  azimuth (Figure 4f) shows a higher suction peak for downwind operation, which corresponds with the higher local torque coefficients in downwind operation. It is not clear why the downwind inboard rotor performance appears to be higher than upwind operations in fully attached flow conditions well away from stall. Potentially, the large rotating root region instrumentation package introduced additional three-dimensional effects and increased inboard radial flow in the upwind configuration, whereas the downwind rotor is affected by the wake of the stationary, streamlined nacelle (Figure 1). [Frau et al. \(2015\)](#) show similar power increases for downwind operation and similar inboard behavior.

Figure 5 shows the difference in average flap bending moment for upwind and downwind operation. The downwind-coned rotor has a tendency to become unconed which produces a flap bending moment opposing the moment from aerodynamic loads. The predicted difference due to coning is 1040 N·m, which compares very well with the measurements. With this setting of downwind coning, the moment becomes negative at low wind speeds.

Blade fatigue is shown in Figure 6, with the damage equivalent load (DEL) for upwind and downwind operation, including downwind with shroud. The DEL was calculated using a rainflow-counting method with MLife ([NWTC Information Portal 2015](#)). Results are shown in the region below stall operation of the turbine. In this region compared to upwind operation, blade fatigue is increased for downwind operation (e.g. 50% increase in DEL at 7 m/s). Use of a tower shroud results in significant reduction in fatigue; however, fatigue loads increase with shroud misalignment (right plot-e.g. 13.5% increase for  $10^\circ$  misalignment at 7 m/s). Here, misalignment is defined as the angle between the freestream velocity and mean chordline of the symmetrical shroud.



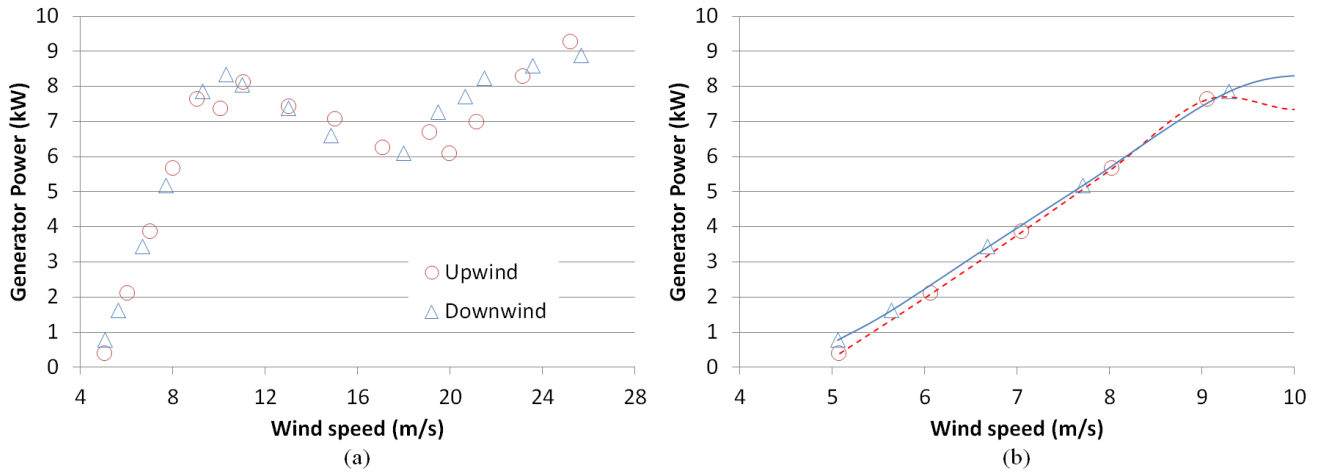


**Figure 3.** Average power for upwind and downwind operation: (a) complete wind speed range, (b) below-rated wind speed. Downwind coning is  $3.4^\circ$ .

Note that operating data was not acquired for  $-10^\circ$  or  $-20^\circ$  misalignment. Causes for these loads are examined below in the wake data study.

Figure 7 and 8 respectively show the azimuth averaged Blade 1 root flap and edge bending moments at 10 m/s and  $0^\circ$  misalignment. The moments have been averaged over 36 revolutions. The blade response is periodic for the loads and configurations shown. The difference in average flap moment due to coning is evident in Figure 7. The edge moments for downwind operation show higher harmonics in Figure 8 compared to the upwind trace, which primarily shows once-per-revolution variation due to the weight vector. The edge loads show periodic excitation from interaction with the tower/shroud wake. The shroud appears to reduce the magnitude of this wake induced mode.

### Tower Wake Data

One of the turbine blades was instrumented with five-hole probes to measure upstream dynamic pressure and flow angle. This blade was fixed in position downwind of the tower to obtain wake measurements. Figure 9 shows the wake velocity normalized to tunnel velocity at three tower diameters downwind and at 7 m/s wind speed. The Reynolds number for this condition is subcritical in the long-established experimental results for cylinder drag. Above this Reynolds number the transition point moves aft and the drag coefficient lowers significantly. A typical  $\cos^2$  tower wake model from the literature (Powles 1983) is shown as well for comparison. The model wake velocity is given by:

$$V_{wake} = V_\infty \left( 1 - d_{wake} \left( \cos^2 \frac{\pi x}{w_{wake}} \right) \right) \quad (1)$$

The comparison with the data is good; however, this model requires knowledge of the maximum wake deficit ( $d_{wake}$ ) and width ( $w_{wake}$ ). These parameters were visually estimated at 0.35 wake deficit and a total wake width of two-diameters.

Figure 10a shows the tower wake velocity normalized to tunnel velocity at 7, 15, and 20 m/s wind speeds. Figure 10b shows at the same speeds the turbulence intensity, defined as the standard deviation of the wake velocity divided by the average tunnel velocity. These speeds represent subcritical, transitional, and supercritical Reynolds numbers for the cylinder wake. The wake deficit and turbulence intensity reduces with Reynolds number and becomes asymmetric. The subcritical wake also shows a double peak in the turbulence intensity. These behaviors were similarly observed in experiments of cylinder wakes by Snyder and Wentz (1981) (this reference should be considered the comprehensive study of wind turbine tower wakes). The double peak was attributed to areas of high mixing in the subcritical wake. The asymmetry was attributed to turbulent separation on one side of the cylinder and laminar separation on the other side. Note that for modern MW-scale turbines, the tower Reynolds number would most likely be supercritical at all operational wind speeds.

Figure 11 shows the spectra of the wake pressure signal at 7 m/s, with a peak at 2.8 Hz. This corresponds to a Strouhal number ( $S = fD/U_\infty$ ) of 0.16. This matches the Strouhal range for subcritical Reynolds numbers as reported in Snyder and Wentz (1981). In contrast to Snyder and Wentz (1981), no peaks were observed in the higher Reynolds number cases. However, Jones (1968) reports on other researchers' work showing no distinct peaks above the critical Reynolds number. Zahle et al. (2009) reports CFD modeling results

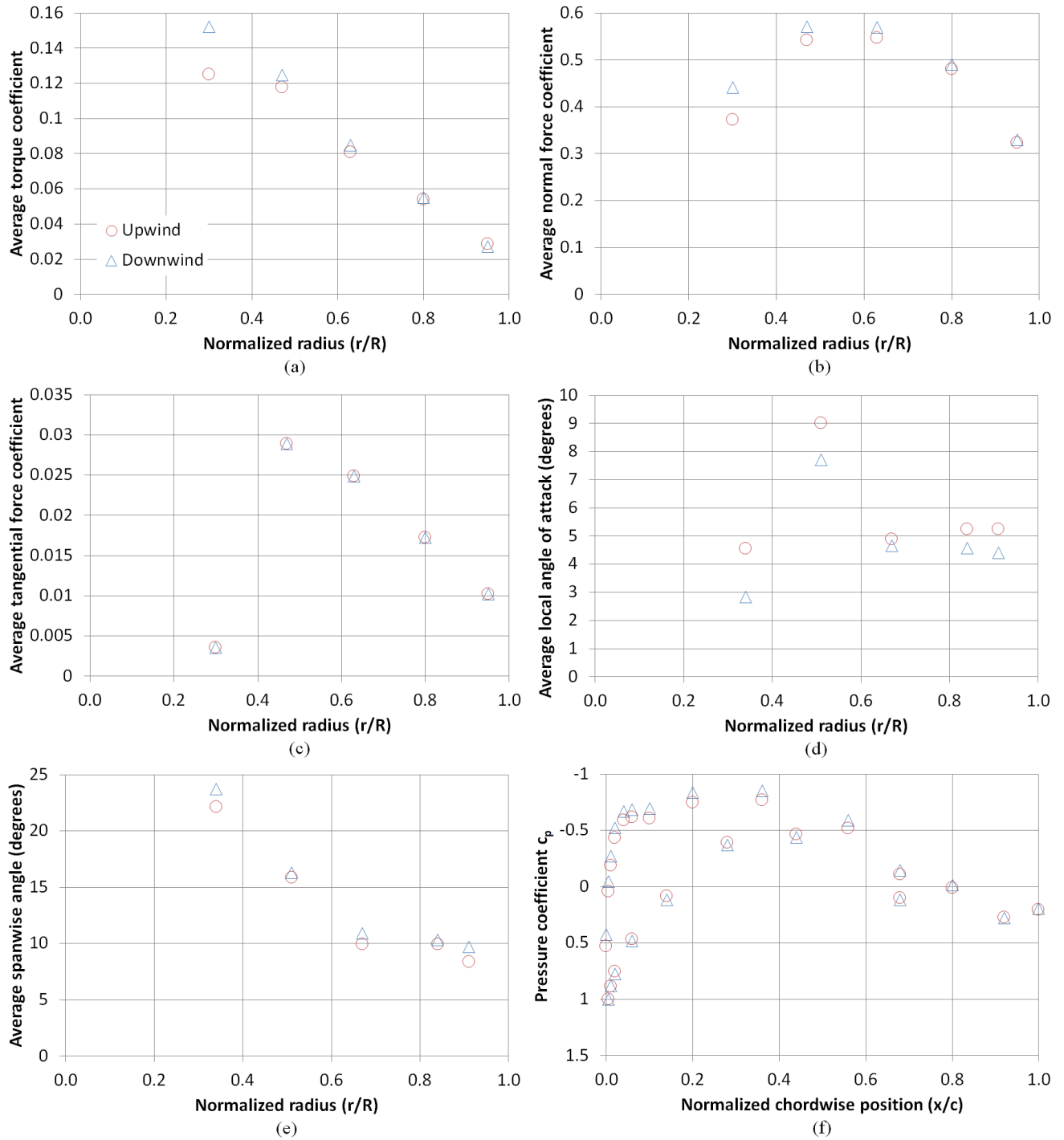


**Figure 4.** 5 m/s data: (a) torque coefficient, (b) normal force coefficient, (c) tangential force coefficient, (d) local flow angle, (e) spanwise flow angle, and (f) pressure coefficient (30% radial station and  $0^\circ$  azimuth)

for tower wake shedding frequencies of 4.1 Hz at 6.7 m/s (Strouhal number 0.24). Although slightly higher than the UAE value, the result is still in the range of typical wake measurements.

Figures 12, 13, and 14 show wake measurements at 7 m/s with the shroud installed and at various misalignment angles. The  $\text{COS}^2$  wake model from Figure 9 is included for comparison. Figure 12 shows the wake with the shroud aligned with the freestream. The average velocity in the wake is actually higher than the freestream (arrow length greater

than 1) where the measurements were taken. Figure 13 shows the shroud misaligned  $\pm 10^\circ$  from the freestream. This  $\pm 10^\circ$  shroud misalignment results in a larger wake deficit than the unshrouded tower configuration. Figure 14 shows the shroud misaligned  $\pm 20^\circ$  from the freestream, with regions of significant reversed flow.

Figure 15a shows the shroud wake velocity normalized to tunnel velocity at 7, 15, and 20 m/s wind speeds for  $0^\circ$  shroud misalignment. Figure 15b shows at the same speeds the turbulence intensity. The wake deficit increases slightly with

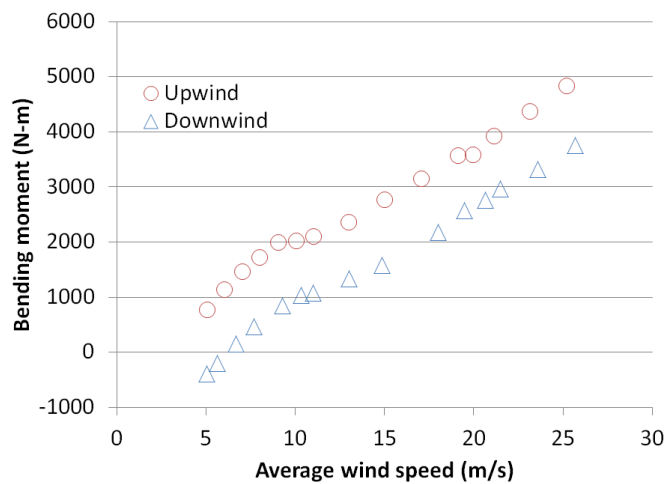


**Figure 5.** Average Blade 1 root flap bending moment for upwind and downwind operation

Reynolds number, and is more narrow than the bare tower wake. These same findings were found in experiments with a tower shroud by [Wilmschurst et al. \(1985\)](#). The turbulence intensity is much lower than the un-shrouded tower wake shown in Figure 10b. No peaks were observed in the spectra of the shroud wake. In summary, the shroud wake is narrower and more steady than the bare tower which has a wider, more fluctuating wake. These results can explain the much lower damage equivalent load in Figure 6 with the shroud installed. Note that tower strakes, tower tapering, or lattice towers could also reduce the tower wake.

Figure 16 and Figure 17 show wake normalized velocity and turbulence intensity for  $\pm 10^\circ$  and  $\pm 20^\circ$  shroud misalignment respectively. With shroud misalignment the wake velocity decreases and turbulence intensity increases dramatically which results in the increased damage equivalent load shown in Figure 6b. These data also show a Reynolds number dependency, especially at the lowest value.

### Effect of Tower Wake on Fatigue

As shown in Figures 7 and 8, the tower and shroud wake result in a periodic load on the blades. To study the effect of the wake on the blade fatigue, the blade was modeled as a single degree-of-freedom spring-mass-damper with periodic forcing from a pulse. The pulse is approximated by a 200-term (harmonics) Fourier series, and the blade response is a linear combination of the response of each harmonic. [Balachandran and Magrab \(2008\)](#) provide example response equations, which are shown in the supplemental material section. The response is linearly based on the pulse (load) magnitude, but is non-linearly related to the ratio of the pulse width (i.e. the wake width) to the period, the damping ratio, and the ratio of the pulse frequency to the blade natural

**Table 2.** Effect of differences in tower and shroud wake on damage equivalent load at 7 m/s nominal freestream wind speed

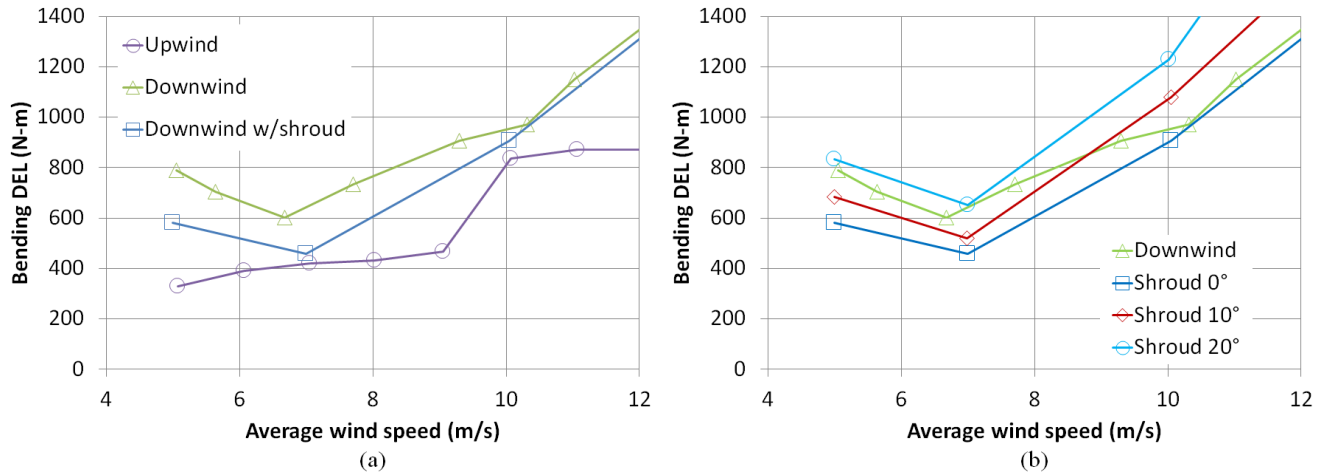
Parameter	Percent Difference
Depth	-15%
Width	-35%
$\zeta = 0.7$ pulse DEL	-11%
$\zeta = 0.05$ pulse DEL	2.3%
Flap DEL	-23%
Edge DEL	2%

frequency. Example 30-second time series were produced for a range of these parameters for values ranging from the UAE to an example 10 MW wind turbine ([Stäblein et al. 2016](#)). And example response is shown in Figure 18.

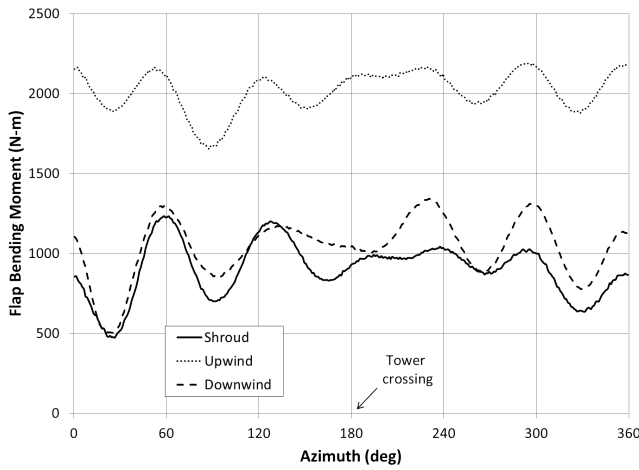
The damage equivalent load was then determined using a rainflow-counting method with MLife ([NWTC Information Portal 2015](#)), because there is no known closed-form DEL solutions for a periodic response. Figure 19 shows the normalized DEL for the pulse excitation as a function of the pulse ratio to the frequency ratio. Figure 19a is for a damping ratio of 0.05, which is representative of blade edge bending. Figure 19b is for a damping ratio of 0.7, which is representative of blade flap bending ([Stäblein et al. 2016](#)). The high damping plot shows increasing load with increasing pulse width and frequency ratio; however, this is not observed in the low damping case.

Figure 20 shows the loading on the outboard portion of the blade resulting from the tower-alone wake and the shroud wake. The difference in width and depth of the wake disturbance and listed in Table 2. As mentioned above for the pulse, the difference in depth would result in a linear difference in DEL. The shroud peak is approximately 15% less than the tower-alone case for both load components. The shroud width is 35% less than the tower-alone case, which results in a different DEL for the pulse case depending on the damping ratio. The DEL is reduced by 11% for a damping ratio of 0.7, which would correspond to flap bending and normal coefficient loading. The DEL is increased 2% for a damping ratio of 0.05, which would correspond to edge bending and tangential coefficient loading. The actual DEL differences are listed at the end of Table 2, which show a decrease in flap bending DEL of 23% and an increase in edge DEL of 2%.

Other features to note about Figure 20 include an initial rise in the loads prior to the drop (minimum). The rise is more pronounced for the bare tower. The recovery after the minimum is similar for the tower and the shroud. Also the shroud minimum is offset from  $180^\circ$ , which may indicate a shroud misalignment or assymetric transition on the shroud.



**Figure 6.** Blade 1 root flap bending moment damage equivalent load (DEL): (a) upwind, downwind, and downwind with shroud, (b) downwind with aligned and misaligned shroud



**Figure 7.** Azimuth averaged Blade 1 root flap moments at 10 m/s wind speed

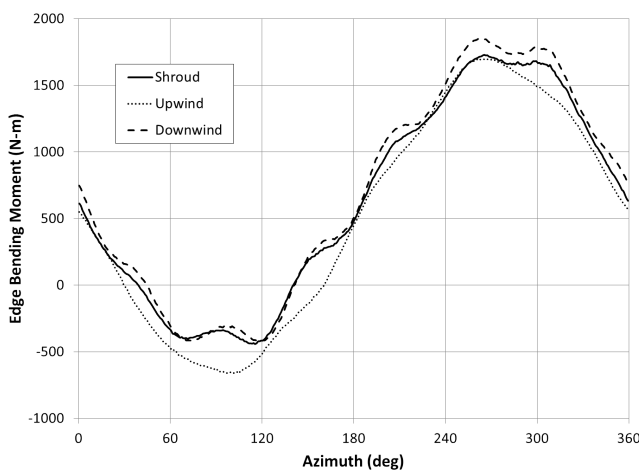


**Figure 8.** Azimuth averaged Blade 1 root edge moments at 10 m/s wind speed

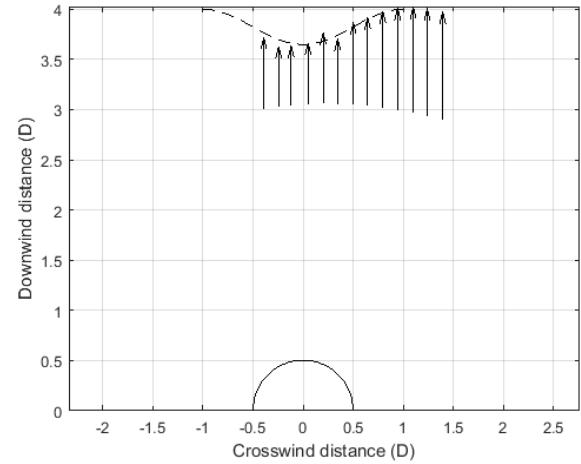


**Figure 9.** Average wake velocity normalized by tunnel velocity (arrows with length according to grid), with  $\cos^2$  wake model (dashes). 7 m/s,  $Re_D = 1.95 \times 10^5$ . Arrow bases are not at same downwind distance due to measurement method.

wake, which is suggested for the tower wake in [Zahle et al. \(2009\)](#). The shroud design would be improved with further knowledge of this coupling. Also note that the time series (not averaged) for Figure 20 is repeatable and does not indicate unsteadiness from the wake itself.

The effect of the shroud on the loads indicate that the primary goal should be to reduce the magnitude of the disturbance. The effect of reducing the width of the wake is more complex; however, if the damping is increased in the edgewise direction (e.g. with tuned mass dampers) the decreased wake width should result in lower loads.

## Conclusions

The comparison between upwind and downwind operation of NREL's Phase VI Unsteady Aerodynamics Experiment show that downwind operation should be reconsidered for future

Also the amount of minimum for the shroud is curious considering the lack of wake depth in Figure 15a. This may indicate a coupling between the rotor and the tower/shroud



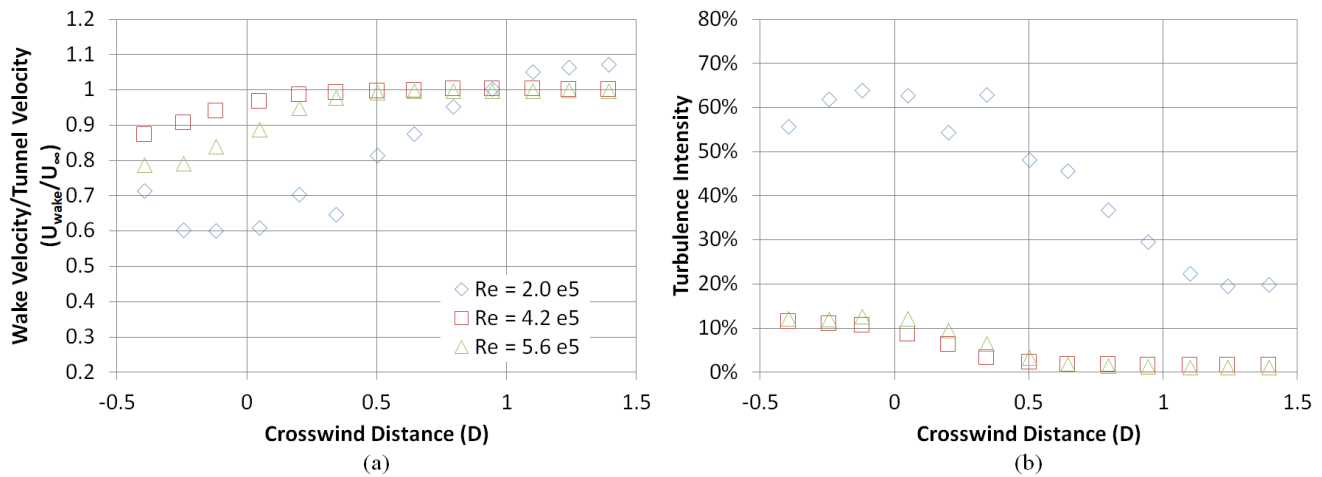


**Figure 10.** (a) tower wake normalized velocity at Reynolds numbers corresponding to 7, 15, and 20 m/s; (b) turbulence intensity at same Reynolds numbers

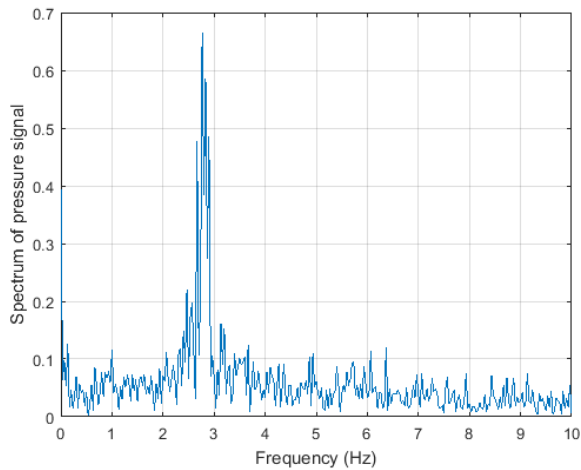


**Figure 11.** Spectra of pressure of 91% 5-hole probe center port in tower wake at 7 m/s

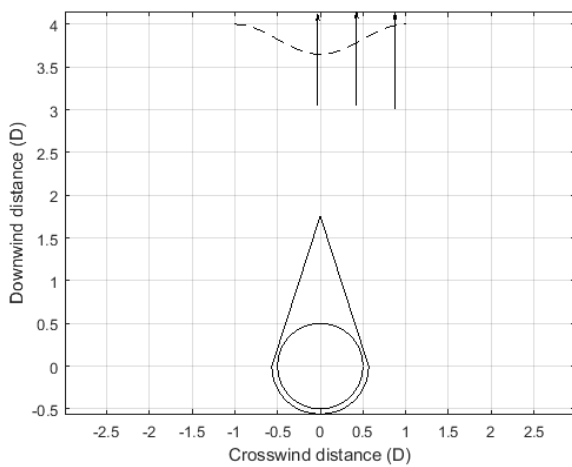


**Figure 12.** Measured normalized wake velocity at 7 m/s with tower shroud at  $0^\circ$  with  $\cos^2$  (dashes) model from Figure 9.  $Re_c = 4.26 \times 10^5$ .

and predictable reduction in average loads for blade flap-bending, in comparison to upwind operation, and does not seem to result in lower energy capture.

The expected increased fatigue loads from downwind operation compared to upwind operation was confirmed in the experiment. The loads are the result of the tower wake, which was measured in this experiment and compare well with previous wake studies. The wake is dependent on the Reynolds numbers encountered in this study. However, the higher, supercritical Reynolds numbers and fully turbulent wakes for large modern turbines may remove this dependency. In regards to the tower wake measurements, the previous research (Snyder and Wentz 1981) should be considered more comprehensive than the UAE measurements.

The fatigue loads in tower wake operation can be mitigated significantly with an aerodynamic shroud. However, the shroud must remain aligned with the wind direction, as the results show fatigue loads returning to tower-alone levels with a  $10^\circ$  misalignment. So a free-yawing wind-vane type shroud or a system tied to the rotor yaw would be required for practical implementation. Further research may demonstrate if a shroud will lower the noise generation.

The Phase VI was machine was stall-regulated with fixed pitch. Future wind tunnel campaigns should consider modern rotor configurations with pitch regulation along with comprehensive rotor wake-measurements.

## Acknowledgements

The authors would like to thank the reviewers of this work for their time and helpful comments. Scott Schreck (formerly of NREL) handled several requests for data. Lee Jay Fingersh of NREL

large wind turbines. Downwind coning offers a significant

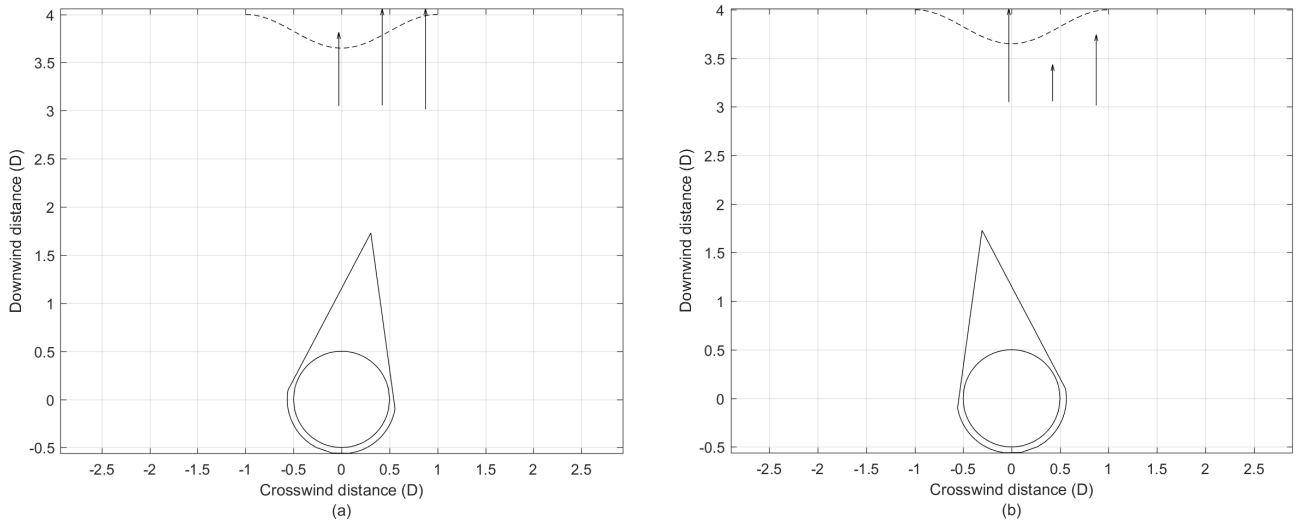


**Figure 13.** Measured normalized wake velocity at 7 m/s with tower shroud at 10° (a) and -10° (b) misalignment with  $\cos^2$  (dashes) model from Figure 9.  $Re_c = 4.26 \times 10^5$ .

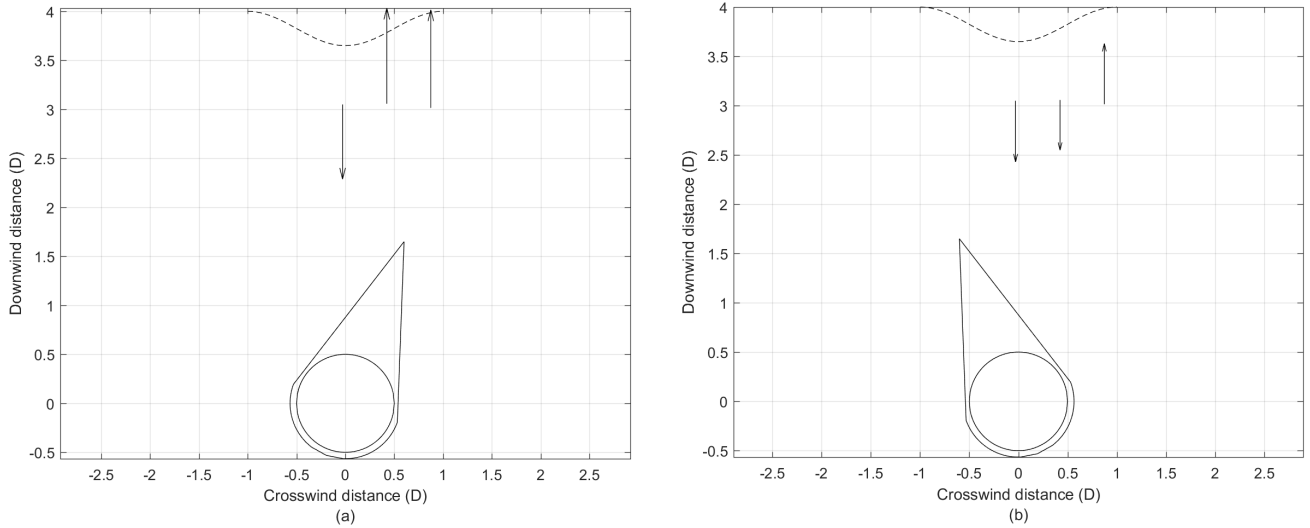


**Figure 14.** Measured normalized wake velocity at 7 m/s with tower shroud at 20° (a) and -20° (b) misalignment with  $\cos^2$  (dashes) model from Figure 9.  $Re_c = 4.26 \times 10^5$ .

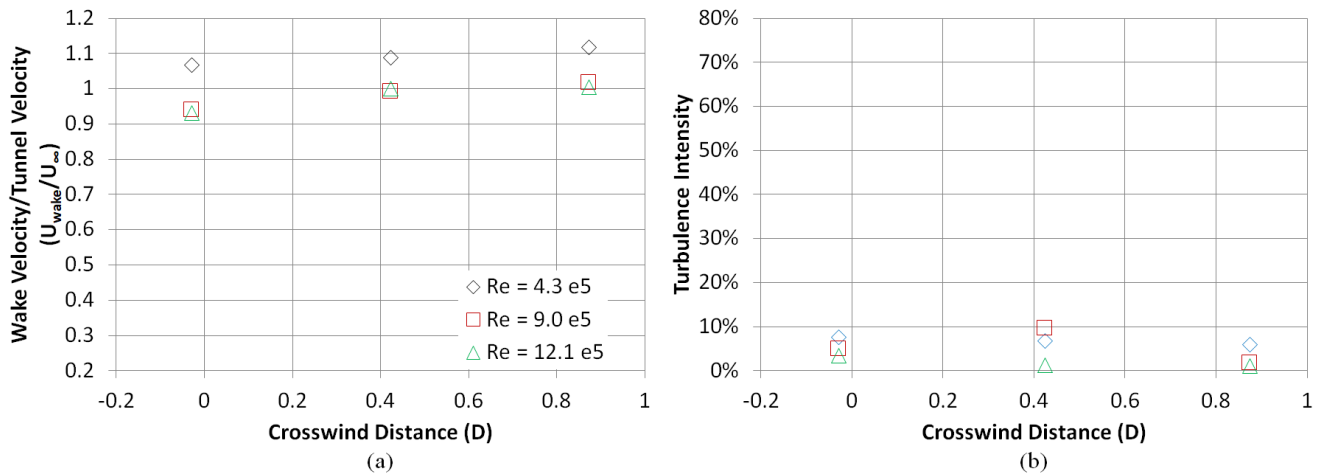


**Figure 15.** (a) tower wake normalized velocity at Reynolds numbers corresponding to 7, 15, and 20 m/s for 0° shroud misalignment; (b) turbulence intensity at same Reynolds numbers

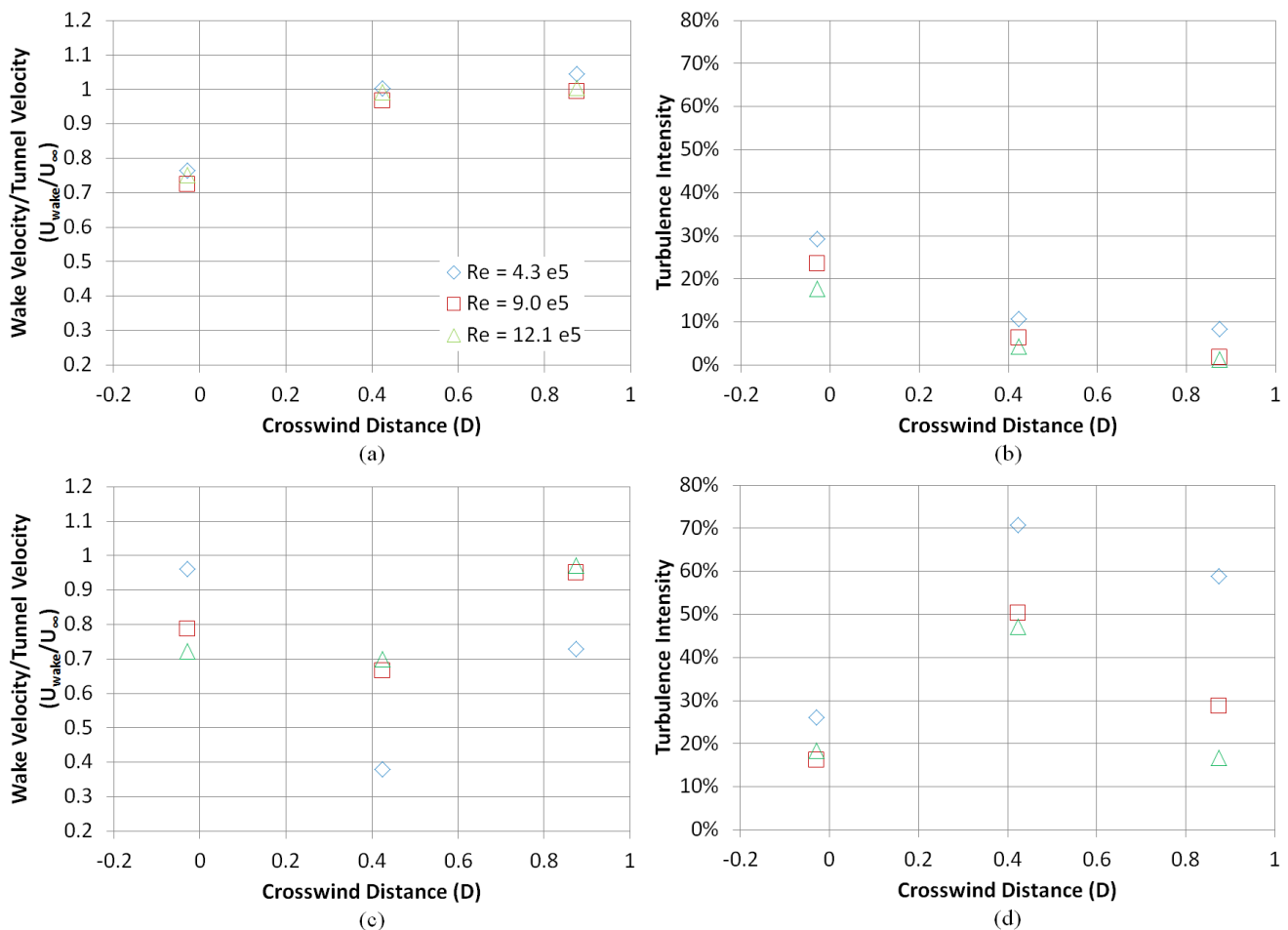


**Figure 16.** Shroud wake normalized velocity (left) and turbulence intensity (right) at chord Reynolds numbers corresponding to 7, 15, and 20 m/s for  $+10^\circ$  (a and b) and  $-10^\circ$  (c and d) shroud misalignment

searched for and provided drawings of the tower shroud. We would also like to thank the entire UAE test team.

Portions of this article were presented at TORQUE 2016: The Science of Making Torque from the Wind (Larwood and Chow 2016).

## References

- Balachandran B and Magrab EB (2008) *Vibrations*. Second edition. CL Engineering.
- Coton FN, Wang T and Galbraith RAM (2002) An examination of key aerodynamic modelling issues raised by the NREL blind comparison. *Wind Energy* 5(2-3): 199–212.
- Frau E, Kress C, Chokani N and Abhari RS (2015) Comparison of performance and unsteady loads of multimewatt downwind and upwind turbines. *Journal of Solar Energy Engineering* 137(84).
- Gipe P (1995) *Wind Energy Comes of Age*. Hoboken, New Jersey, U.S.A.: John Wiley & Sons, Inc.
- Glasgow JC, Miller DR and Corrigan RD (1981) Comparison of Upwind and Downwind Rotor Operations of the DOE/NASA 100-kW MOD-0 Wind Turbine. In: Thresher RW (ed.) *Wind Turbine Dynamics*, NASA-CP-2185. Cleveland, Ohio: NASA, pp. 225–234.
- Hand MM, Simms DA, Fingersh, L J DW Jager, Cotrell JR, Schreck S and Larwood SM (2001) *Unsteady Aerodynamics Experiment Phase VI: Wind Tunnel Test Configurations and Available Data Campaigns*. NREL/TP-500-29955. Golden, CO: National Renewable Energy Laboratory.
- Ichter B, Steele A, Loth E, Moriarty P and Selig M (2016) A morphing downwind-aligned rotor concept based on a 13-mw wind turbine. *Wind Energy* 19(4): 625–637.
- Jones GWJ (1968) Unsteady lift forces generated by vortex shedding about a large, stationary, and oscillating cylinder at high reynolds numbers. NASA-TM-X-61214, NASA Langley Research Center,.
- Kress C, Chokani N and Abhari R (2015) Downwind wind turbine yaw stability and performance. *Renewable Energy* 83: 1157 – 1165.
- Larwood SM and Chow R (2016) Comparison of upwind and downwind operation of the nrel phase vi experiment. *Journal of Physics: Conference Series* 753(2): 022041.

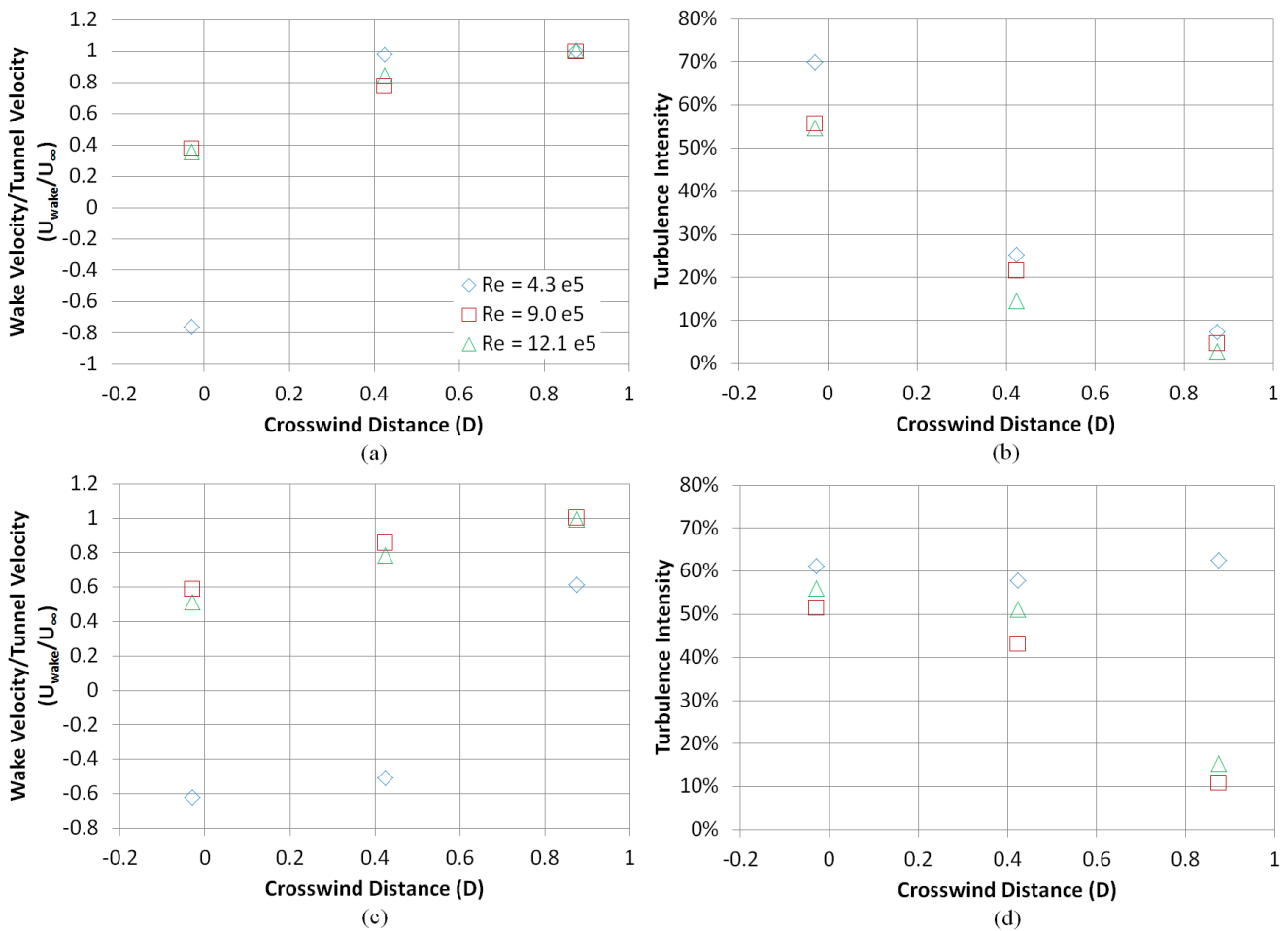


**Figure 17.** Shroud wake normalized velocity (left) and turbulence intensity (right) at chord Reynolds numbers corresponding to 7, 15, and 20 m/s for  $+20^\circ$  (a and b) and  $-20^\circ$  (c and d) shroud misalignment

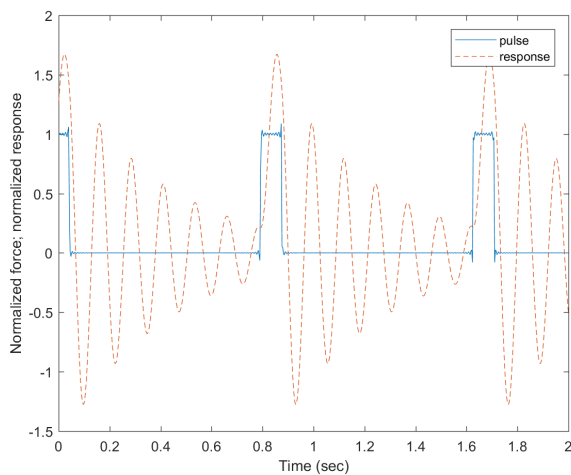


**Figure 18.** Example pulse (200 harmonics) response for 0.15 frequency ratio, 0.1 pulse ratio, and damping  $\zeta = 0.05$

Loth E, Steele A, Qin C, Ichter B, Selig MS and Moriarty P (2017) Downwind pre-aligned rotors for extreme-scale wind turbines. *Wind Energy* DOI:10.1002/we.2092.

NWTC Information Portal (2015) (MLife). <https://nwtc.nrel.gov/MLife>. Last modified 30-October-2015 ;

Accessed 19-April-2017.

O'Connor KO, Loth E and Selig MS (2013) Design of a 2-d fairing for a wind turbine tower. In: *31st AIAA Applied Aerodynamics Conference*.

O'Connor KO, Loth E and Selig MS (2015) Experiments on fairing design for a wind turbine tower. In: *AIAA SciTech 2015*.

Powles SRJ (1983) The effects of tower shadow on the dynamics of a horizontal-axis wind turbine. *Wind Engineering* 7: 26–42.

Simms D, Schreck S, Hand M and Fingersh L (2001) *NREL Unsteady Aerodynamics Experiment in the NASA-Ames Wind Tunnel: A Comparison of Predictions to Measurements*. NREL/TP-500-29494. Golden, CO: National Renewable Energy Laboratory.

Simms D, Schreck S, Hand M, Fingersh L, Cotrell J, Pierce K and Robinson M (1999) *Plans for Testing the NREL Unsteady Aerodynamics Experiment 10m Diameter HAWT in the NASA Ames Wind Tunnel*. NREL/TP-500-27599. Golden, CO: National Renewable Energy Laboratory.

Snyder MH and Wentz WH (1981) Dynamics of wakes downstream of wind turbine towers. In: Thresher RW (ed.) *Wind Turbine*



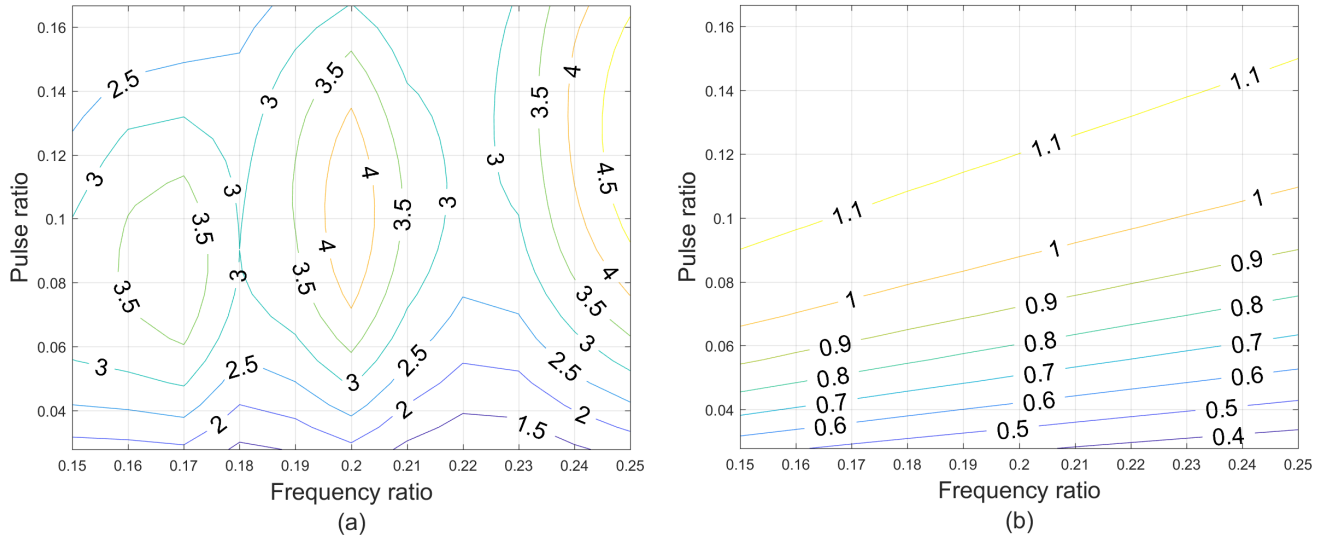


**Figure 19.** Damage equivalent load for pulse excitation as function of width of pulse to period (pulse ratio) and ratio of pulse frequency to natural frequency for damping ratio of 0.05 (a) and 0.7 (b)

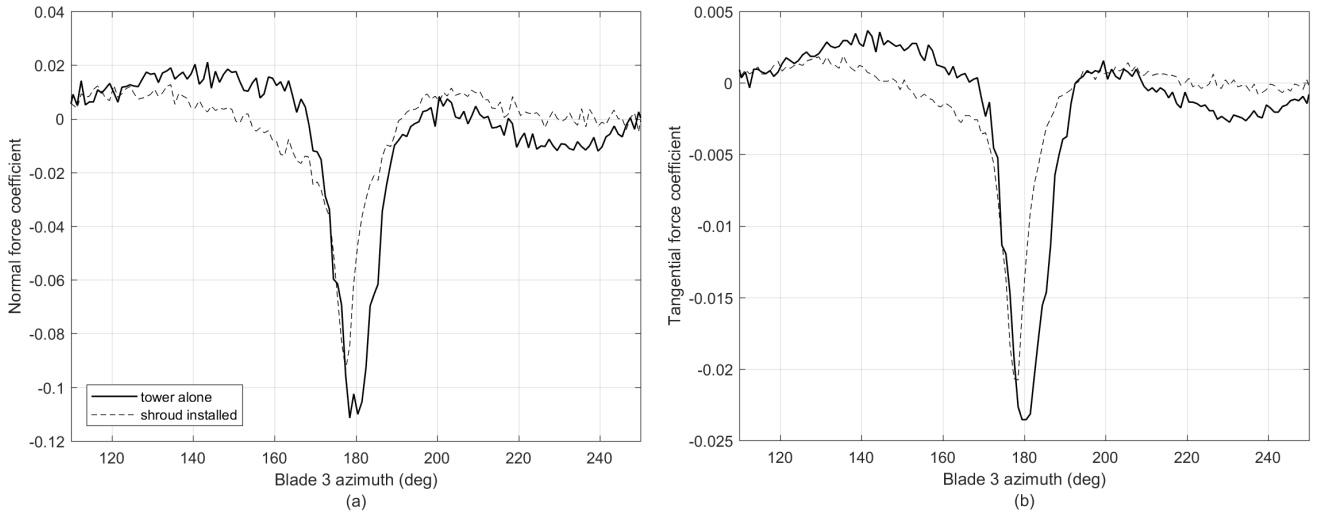


**Figure 20.** Azimuth-averaged and mean-removed normal force coefficient (a) and tangential force coefficient (b) at 95% station at 7 m/s nominal freestream wind speed.

*Dynamics*, NASA-CP-2185. Cleveland, Ohio: NASA, pp. 225–234.

Spera D (2009) *Wind Turbine Technology: Fundamental Concepts of Wind Turbine Engineering*. New York, NY: ASME Press.

Ståblein AR, Hansen MH and Verelst DR (2016) Modal properties and stability of bend-twist coupled wind turbine blades. *Wind Energy Science Discussions* 2016: 1–27.

Wilmshurst SMB, Powles SJR and A WD (1985) The problem of tower shadow. In: Garrad A (ed.) *Wind energy conversion, 1985: proceedings of the 7th British Wind Energy Association Conference*. London: Mechanical Engineering Publications Ltd, pp. 95–102.

Yoshida S (2006) Performance of downwind turbines in complex terrains. *Wind Engineering* 30(6): 487–502.

Zahle F, Sørensen NN and Johansen J (2009) Wind turbine rotor-tower interaction using an incompressible overset grid method. *Wind Energy* 12(6): 594–619.

### Supplemental material

A periodic function can be represented by the Fourier series (Balachandran and Magrab 2008):

$$f(t) = \frac{a_0}{2} + \sum_{i=1}^{\infty} [a_i \cos(i\omega_0 t) + b_i \sin(i\omega_0 t)] \quad (2)$$

where  $\omega_0$  is the fundamental frequency, and  $a_i$ ,  $b_i$  are the Fourier amplitudes, given by:

$$a_i = \frac{2}{T} \int_0^T f(t) \cos(i\omega_0 t) dt \quad i = 0, 1, 2, \dots \quad (3)$$

$$b_i = \frac{2}{T} \int_0^T f(t) \sin(i\omega_0 t) dt \quad i = 0, 1, 2, \dots \quad (4)$$

where  $T = 2\pi/\omega_0$  is the period. The steady-state response is a summation of responses to individual harmonics, given by:

$$x(\tau) = \frac{1}{k} \left[ c_0 + \sum_{i=1}^{\infty} c_i(\Omega_i) \sin(\Omega_i \tau - \theta(\Omega_i) + \psi_i) \right] \quad (5)$$

where  $\tau = \omega_n t$ ,  $k$  is the system stiffness,  $\Omega_i = i\omega_0/\omega_n$  where  $\omega_n$  is the natural frequency of the system, and the various phases and coefficients given by:

$$\begin{aligned} c_0 &= \frac{a_0}{2} \\ c_i &= H(\Omega_i) \sqrt{a_i^2 + b_i^2} \\ \theta(\Omega_i) &= \tan^{-1} \frac{2\zeta\Omega_i}{1 - \Omega_i^2} \\ H(\Omega_i) &= \frac{1}{\sqrt{(1 - \Omega_i^2)^2 + (2\zeta\Omega_i)^2}} \\ \psi_i &= \tan^{-1} \frac{a_i}{b_i} \end{aligned} \quad (6)$$

A periodic pulse train can be represented by the Fourier series:

$$f(t) = F_0 \alpha \left[ 1 + 2 \sum_{i=1}^{\infty} \frac{\sin(i\pi\alpha)}{(i\pi\alpha)} \cos(2i\pi t/T) \right] \quad (7)$$

where  $F_0$  is the peak level of the pulse and  $\alpha = t_d/T$  is the width of the pulse ( $t_d$ ) divided by the period. Further normalization gives:

$$f(\tau) = F_0 \alpha \left[ 1 + 2 \sum_{i=1}^{\infty} \frac{\sin(i\pi\alpha)}{(i\pi\alpha)} \cos(\Omega_i \tau) \right] \quad (8)$$

Comparing to Equation 2:

$$\frac{a_0}{2} = \alpha F_0; \quad b_i = 0; \quad a_i = 2\alpha F_0 \frac{\sin(i\pi\alpha)}{i\pi\alpha} \quad (9)$$

Inserting the above into Equation 5 for the steady-state response of a single degree-of-freedom system to a pulse train:

$$x(\tau) = \frac{\alpha F_0}{k} \left[ 1 + 2 \sum_{i=1}^{\infty} c_i(\Omega_i) \sin(\Omega_i \tau - \theta(\Omega_i) + \psi_i) \right] \quad (10)$$

with amplitude:

$$c(\Omega_i) = \frac{1}{\sqrt{(1 - \Omega_i^2)^2 + (2\zeta\Omega_i)^2}} \left| \frac{\sin(i\pi\alpha)}{i\pi\alpha} \right| \quad (11)$$

**Table 3.** Shroud coordinates centered at the tower, symmetric about  $y$ -axis, and normalized by tower diameter (0.4064 m).

$x$	$y$
-0.607797732	0.003921446
-0.604799819	0.043064516
-0.59635345	0.085892803
-0.586239061	0.120094921
-0.572418763	0.15703316
-0.558659401	0.187551424
-0.546820756	0.210438514
-0.52314754	0.249993372
-0.494357884	0.290607571
-0.468632545	0.321929242
-0.430806774	0.361677902
-0.390658743	0.397624226
-0.354685211	0.425440845
-0.309069784	0.455744359
-0.266527965	0.479753935
-0.220273123	0.501797741
-0.172848081	0.520458734
-0.118705731	0.537295861
-0.060337081	0.550413864
0.006913433	0.559324911
0.074122419	0.561829841
0.137923745	0.558241808
0.207025794	0.548110513
0.256979762	0.537295861
0.320348913	0.520458734
0.381729669	0.501797741
0.43087007	0.4855701
0.4880163	0.46557109
0.549276301	0.443075868
0.598070504	0.42454934
0.643273727	0.406997591
0.708830425	0.381040581
0.778295706	0.353114632
0.855165406	0.321929242
0.917401515	0.296558649
0.982295112	0.270011643
1.049414334	0.242445673
1.119401136	0.213530058
1.201979942	0.179204976
1.251123079	0.158717877
1.311377914	0.133541604
1.381638166	0.104144304
1.441458335	0.079052211
1.50896741	0.050675405
1.5823042	0.01920261